Cellular/Molecular

A Mechanism Intrinsic to the Vesicle Fusion Machinery Determines Fast and Slow Transmitter Release at a Large CNS Synapse

Markus Wölfel,[1] Xuelin Lou,[1] and Ralf Schneggenburger[1,2]

[1]AG Synaptic Dynamics and Modulation, Department of Membrane Biophysics, Max-Planck-Institut für Biophysikalische Chemie, Am Fassberg 11, D-37077 Göttingen, Germany, and [2]Laboratory of Synaptic Mechanisms, Brain-Mind Institute, École Polytechnique Fédérale de Lausanne, CH-1015 Lausanne, Switzerland

Heterogeneity of release probability *p* between vesicles in the readily releasable pool (RRP) is expected to strongly influence the kinetics of depression at synapses, but the underlying mechanism(s) are not well understood. To test whether differences in the intrinsic Ca^{2+} sensitivity of vesicle fusion might cause heterogeneity of *p*, we made presynaptic Ca^{2+}-uncaging measurements at the calyx of Held and analyzed the time course of transmitter release by EPSC deconvolution. Ca^{2+} uncaging, which produced spatially homogeneous elevations of $[Ca^{2+}]_i$, evoked a fast and a slow component of release over a wide range of $[Ca^{2+}]_i$, showing that mechanism(s) intrinsic to the vesicle fusion machinery cause fast and slow transmitter release. Surprisingly, the number of vesicles released in the fast component increased with Ca^{2+}-uncaging stimuli of larger amplitudes, a finding that was most obvious below ~10 μM $[Ca^{2+}]_i$ and that we call "submaximal release" of fast-releasable vesicles. During trains of action potential-like presynaptic depolarizations, submaximal release was also observed as an increase in the cumulative fast release at enhanced release probabilities. A model that assumes two separate subpools of RRP vesicles with different intrinsic Ca^{2+} sensitivities predicted the observed Ca^{2+} dependencies of fast and slow transmitter release but could not fully account for submaximal release. Thus, fast and slow transmitter release in response to prolonged $[Ca^{2+}]_i$ elevations is caused by intrinsic differences between RRP vesicles, and an "a posteriori" reduction of the Ca^{2+} sensitivity of vesicle fusion after the onset of the stimulus might cause submaximal release of fast-releasable vesicles and contribute to short-term synaptic depression.

Key words: **synapse; vesicle; Ca^{2+}; Ca^{2+} sensor; readily releasable pool; short-term plasticity**

Introduction

During synaptic transmission, release of neurotransmitter is supported from a pool of docked and fusion-competent vesicles that can be defined functionally as the readily releasable pool (RRP) of vesicles (Schikorski and Stevens, 2001; Sorensen, 2004). In recent years, a heterogeneity of release probability has received considerable attention, because it has become apparent that some RRP vesicles are released more reluctantly than others. At the calyx of Held, a large glutamatergic synapse in the brainstem, vesicles newly recruited to the RRP have an initially low release probability (Wu and Borst, 1999), and prolonged presynaptic voltage-clamp depolarizations lead to a fast and a slow phase of transmitter release that correspond to rapidly and more reluctantly releasable vesicles, respectively (Sakaba and Neher, 2001a,b). Evidence for reluctantly releasable vesicles has also been obtained at hippocampal synapses, in which an apparent increase in pool size was observed upon increasing the release probability, indicating that reluctant vesicles only contribute to transmission at elevated release probability (Moulder and Mennerick, 2005). Heterogeneity of *p* is expected to strongly influence the synaptic strength during repetitive stimulation (Trommershäuser et al., 2003) and is therefore an important factor shaping short-term plasticity of synaptic transmission.

The mechanism(s) that cause heterogeneity in release probability *p* between readily releasable vesicles are, however, not well understood. Two possible explanations immediately arise. First, a differential colocalization of RRP vesicles with presynaptic Ca^{2+} channels might cause a heterogeneity of *p*. Vesicles located closer to Ca^{2+} channel(s) are expected to experience a higher intracellular Ca^{2+} signal than those located at larger distances (Meinrenken et al., 2002) (for review, see Neher, 1998). Evidence for such a "positional heterogeneity" has come from the finding that, in some synapses, the slow Ca^{2+} buffer EGTA blocks part but not all of the release triggered by brief stimuli (Borst and Sakmann,

Received Oct. 13, 2006; revised Feb. 9, 2007; accepted Feb. 10, 2007.

This work was supported by the Deutsche Forschungsgemeinschaft (Sonderforschungsbereich-406 TP B1 and Schn451/4-1 and a Heisenberg Fellowship to R.S.). We thank Felix Felmy, Stefan Hallermann, Erwin Neher, Takeshi Sakaba, and Holger Taschenberger for critical comments on a previous version of this manuscript.

Correspondence should be addressed to Dr. Ralf Schneggenburger, Laboratory of Synaptic mechanisms École Polytechnique Fédérale de Lausanne, Brain Mind Institute, Bâtiment AAB, Station 15, CH-1015 Lausanne, Switzerland. E-mail: ralf.schneggenburger@epfl.ch.

M. Wölfel's present address: Department of Cell Biology, Yale University School of Medicine, New Haven, CT 06520-8002.

X. Lou's present address: Howard Hughes Medical Institute, Yale University School of Medicine, New Haven, CT 06520-8002.

DOI:10.1523/JNEUROSCI.4471-06.2007

 0270-6474/07/273198-13$15.00/0

1996; Rozov et al., 2001), implying that some readily releasable vesicles are located closer to Ca^{2+} channels than others (Burrone et al., 2002; Meinrenken et al., 2002). The second possibility is that the Ca^{2+} sensitivity of vesicle fusion is different among RRP vesicles, but this possibility has not been addressed at synapses. In chromaffin cells, Ca^{2+} uncaging, which leads to a spatially uniform elevation of the intracellular Ca^{2+} concentration ($[Ca^{2+}]_i$), induces a fast and a slow component of exocytosis (Heinemann et al., 1994; Voets, 2000), likely indicating the existence of two subpools of readily releasable vesicles with distinct Ca^{2+} sensitivities (for review, see Sorensen, 2004).

To investigate whether intrinsic differences exist between RRP vesicles at a CNS synapse, we applied Ca^{2+} uncaging at the calyx of Held (Bollmann et al., 2000; Schneggenburger and Neher, 2000) and analyzed the resulting time course of transmitter release. We found that Ca^{2+} uncaging induced fast and slow transmitter release over a wide range of $[Ca^{2+}]_i$, indicating that the difference between fast and slowly releasable vesicles is primarily attributable to a mechanism intrinsic to the vesicle fusion machinery. We also observed, however, that the number of vesicles released in the fast release component increases with Ca^{2+}-uncaging stimuli of increasing amplitudes, a finding that we call "submaximal release" of a fast-releasable pool (FRP). These findings indicate that, besides depletion of well separable (sub)pools of readily releasable vesicles, other mechanisms, such as an "a posteriori" reduction of Ca^{2+} sensitivity after the onset of a Ca^{2+} stimulus, could explain heterogeneity of release probability during synaptic depression.

Materials and Methods

Slice preparation and solutions. Slices, 200 μm thick, containing the medial nucleus of the trapezoid body made from 8- to 10-d-old Wistar rats, similar to the method described previously (Schneggenburger et al., 1999). Slices were stored in a chamber with extracellular solution containing the following (in mM): 125 NaCl, 25 $NaHCO_3$, 2.5 KCl, 1.25 NaH_2PO_4, 1 $MgCl_2$, 2 $CaCl_2$, 25 glucose, 0.4 ascorbic acid, 3 myo-inositol, and 2 Na-pyruvate, pH 7.4 (when bubbled with 95% O_2–5% CO_2). During recordings, TTX (1 μM), tetraethylammonium (TEA) (10 mM), D-APV (50 μM), cyclothiazide (CTZ) (100 μM), and γ-D-glutamylglycine (γ-DGG) (2 mM) were also present. The pipette solution for postsynaptic recordings contained the following (in mM): 130 Cs-gluconate, 20 TEA-Cl, 20 HEPES, 5 EGTA, 5 Na_2-phosphocreatine, 4 MgATP, and 0.3 Na_2GTP. The presynaptic pipette solution for Ca^{2+} uncaging experiments contained the following (in mM): 130 Cs-gluconate, 20 TEA-Cl, 20 HEPES, 5 Na_2ATP, 0.3 Na_2GTP, 0.1 fura-2FF, 1.5 (or sometimes 3 mM) DM-nitrophen, 1.3 (or sometimes 2.4 mM) $CaCl_2$, 0.5 (1.0) $MgCl_2$. For paired recordings without Ca^{2+} uncaging (see Figs. 2, 7), the presynaptic pipette solution contained the following (in mM): 130 Cs-gluconate, 20 TEA-Cl, 20 HEPES, 0.2 EGTA, 5 Na_2-phosphocreatine, 4 MgATP, and 0.3 Na_2GTP.

Electrophysiological recordings. For whole-cell patch-clamp recordings, an EPC-9/2 patch-clamp amplifier (HEKA Elektronik, Lambrecht/Pfalz, Germany) was used. Currents were sampled at 50 kHz using the software Pulse (version 8.50; HEKA Elektronik) and processed with the analysis software Igor Pro (WaveMetrics, Lake Oswego, OR). The holding potential was −80 and −70 mV for presynaptic and postsynaptic recordings, respectively. Presynaptic membrane capacitance was measured with the sine + DC method (Lindau and Neher, 1988), using the lock-in extension of the Pulse software, with a 2 kHz, 70 mV peak-to-peak sine wave as described previously (Wölfel and Schneggenburger, 2003). The amplitude of the membrane capacitance (C_m) jump was taken as the time average over 30 ms, at 50–100 ms after the repolarization. This was necessary because, at earlier times, a relaxation of C_m traces was observed that can be attributed to artifacts caused by the depolarizing pulse (see Fig. 2*B*) (Wölfel and Schneggenburger, 2003; Yamashita et al., 2005).

Patch pipettes had resistances of 2.5–3.5 and 4.0–5.5 MΩ for presynaptic and postsynaptic recordings, respectively. The series resistance (R_S) during whole-cell recordings was compensated by 50% for presynaptic and by 50–90% for postsynaptic recordings (time constant of 10 μs), using the R_S compensation circuit of the EPC-9. Remaining R_S errors were compensated by an off-line routine (Meyer et al., 2001). Off-line compensation usually increased the peak EPSC amplitudes by <50%; if the increase was larger, the data were discarded. The postsynaptic recordings were made at the lowest amplification (0.5 mV/pA) of the intermediate gain range of the EPC-9 amplifier. We observed that, with an R_S compensation setting of 80% (a typical value), the current output beyond 15 nA rose with an ~2.5-fold reduced amplification, before the current output saturated at 20 nA. This led to a distortion of the peak EPSCs around the last 1–2 nA in a few of our recordings with Ca^{2+} steps >20 μM (see Fig. 5*A2*, black trace). We did not further correct for this effect. If we had corrected for it, a slightly larger fast release component would have resulted in these cases.

Ca^{2+} uncaging and $[Ca^{2+}]_i$ imaging. Ca^{2+} was uncaged from Ca^{2+}-loaded DM-nitrophen using a fast flash lamp (model SP 20; Rapp Optoelectronic, Hamburg, Germany). The flash light intensity followed a Gaussian time course with 0.2 ms half-width, and simulations showed that the peak $[Ca^{2+}]_i$ was reached within 0.6 ms. The intracellular Ca^{2+} concentration, $[Ca^{2+}]_i$, was measured with the ratiometric Ca^{2+} indicator dye fura-2FF excited by light of 350 and 380 nm wavelengths, supplied by a monochromator (T.I.L.L. Photonics, Gräfelfing, Germany). Fluorescent images were obtained with an interline-transfer 480 × 640 pixel CCD, controlled by the software Tillvision (T.I.L.L. Photonics). Images were binned by 8 × 15, resulting in a pixel size of 1.32 × 2.48 μm in the object plane with the standardly used 60× objective (Olympus Optical, Tokyo, Japan). A single or sometimes two 350/380 nm image pairs were taken before the flash. At 3–4 ms after the flash, imaging was resumed by taking a fast series of four 380 nm images, followed by another series of 350/380 nm images. The exposure time was 5 ms.

The flash light intensity was attenuated by neutral density filters (transmittance of 10, 32, or 50%) to produce $[Ca^{2+}]_i$ steps of different amplitudes. For most experiments, the flash light and the monochromator light were combined into the epifluorescence condenser by using a sapphire window, which admitted 85% of the flash light and 15% of the monochromator light, respectively. For the experiments in Figure 5, we attempted to slow the decay of $[Ca^{2+}]_i$ by admitting an increased intensity of monochromator light (60%), by using a 60–40% beam splitter (Rapp Optoelektronik, Hamburg, Germany) and increasing the DM-nitrophen concentration to 3 mM. The resulting increased photolysis rate by the monochromator light partially compensated for the cellular Ca^{2+} extrusion and thereby slowed the decay of $[Ca^{2+}]_i$.

Images were analyzed off-line in Tillvision, and the resulting time series of fluorescence intensities of several pixels and the background fluorescence of a small area next to the calyx were transferred to Igor Pro (WaveMetrics) for additional analysis. $[Ca^{2+}]_i$ was calculated from the background-corrected fluorescence ratio at 350 and 380 nm wavelengths (Grynkiewicz et al., 1985), after obtaining the necessary calibration constant as described previously (Schneggenburger, 2004).

Spatial homogeneity of Ca^{2+} uncaging. An important assumption for testing the intrinsic heterogeneities in the Ca^{2+} sensitivity between RRP vesicles in Ca^{2+}-uncaging experiments is the spatial homogeneity of $[Ca^{2+}]_i$ elevations produced by Ca^{2+} uncaging. We verified the spatial homogeneity by analyzing the variability of post-flash $[Ca^{2+}]_i$ values between adjacent binned pixels along the length of the calyx (Fig. 1). In the example of Figure 1*A–C*, the measured variability of peak $[Ca^{2+}]_i$ values between the pixels was 0.04, when expressed as coefficient of variation (SD/mean). The peak $[Ca^{2+}]_i$ values were independent from the distance of the pixel from the pipette tip (Fig. 1*C*,*D*), excluding a systematic bias toward smaller post-flash $[Ca^{2+}]_i$ signals with increasing distance. Such a bias might, in theory, occur if the Ca^{2+}-loading state of DM-nitrophen were significantly different with increasing distance from the tip of the whole-cell pipette. The coefficient of variation (c.v.) of $[Ca^{2+}]_i$ between individual pixels was on average 0.07 ± 0.02 (n = 14 flashes).

We further checked whether the (small) spatial heterogeneity of post-

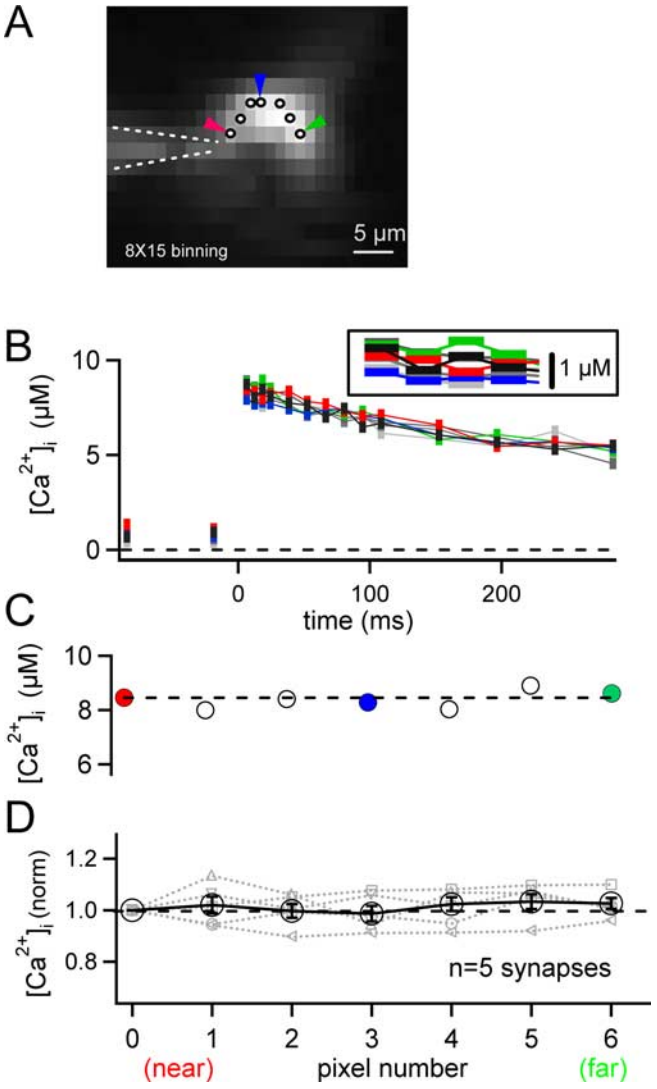

Figure 1. Spatial homogeneity of $[Ca^{2+}]_i$ elevations produced by Ca^{2+} uncaging. ***A***, Fluorescence image at 380 nm excitation wavelength of a calyx of Held during Ca^{2+} uncaging. Pixel binning, 8 × 15; exposure time, 5 ms. The (binned) pixels used for analysis of $[Ca^{2+}]_i$ are indicated by circles, and the arrowheads in colors point to pixels located at increasing distances from the tip of the presynaptic pipette. ***B***, $[Ca^{2+}]_i$ resulting from ratiometric measurements for a single flash, analyzed separately for the individual pixels shown in ***A***. The four $[Ca^{2+}]_i$ measurements immediately after the flash are shown enhanced in the inset. Same color code as in ***A***. ***C***, Plot of the peak $[Ca^{2+}]_i$ as a function of pixel number, sorted according to the distance of the pixels from the pipette tip. The coefficient of variation of peak $[Ca^{2+}]_i$ between neighboring pixels was 0.04 in this cell. ***D***, Peak $[Ca^{2+}]_i$ values from $n = 5$ similar measurements (gray symbols), normalized to the amplitude of the first (nearest) pixel of each measurement. The average data are also shown (black symbols). Note that post-flash $[Ca^{2+}]_i$ amplitudes are constant with increasing distance from the tip of the pipette.

flash $[Ca^{2+}]_i$ was spatially random or whether the same pixels consistently reported relatively higher (or lower) $[Ca^{2+}]_i$ for repeated flashes. We subtracted the spatially averaged $[Ca^{2+}]_i$ value from the $[Ca^{2+}]_i$ value measured in each pixel and plotted these differential $[Ca^{2+}]_i$ values as a function of flash number (data not shown), for all cells in which several flashes with the same light intensity were applied sequentially. For two cells, there were no pixels that consistently reported high or low $[Ca^{2+}]_i$ values with repeated flashes. In another cell, there was some positive correlation for the differential $[Ca^{2+}]_i$ values over two flashes. It is possible, therefore, that part of the $[Ca^{2+}]_i$ variability is caused by a true difference in $[Ca^{2+}]_i$ between pixels, but most of the apparent spatial variability probably arises because of (spatially random) measurement noise. In the simulations (see Fig. 6*E*,*F*), we always modeled Ca^{2+}-uncaging-evoked release assuming a variable $[Ca^{2+}]_i$ signal with a c.v. of 0.07, equal to the measured average value. The variability of $[Ca^{2+}]_i$ used in the models can thus be regarded as a worst-case simulation.

In addition, we determined the homogeneity of flash-light illumination in the *z*-direction by using dextran-bound 4,5-dimethoxy-2-nitrobenzyl–FITC in a gel block and liberating FITC by flash-light discharges in the same way as during Ca^{2+} uncaging. The resulting fluorescence measurements of uncaged FITC showed that, within 20 μm above and below the focal plane, the flash illumination intensity dropped by <0.1%. Thus, flashes illuminated the calyx homogeneously over a depth of at least ±20 μm, and we therefore assume that the resulting $[Ca^{2+}]_i$ increase was also homogeneous along the *z*-axis.

Data analysis. All recorded currents were analyzed in Igor Pro software (WaveMetrics). Presynaptic Ca^{2+} currents were corrected for capacitative and leak currents with a P/4 protocol. The time course of quantal release rates were calculated by EPSC deconvolution (Neher and Sakaba, 2001). To reduce the influence of AMPA-receptor desensitization and saturation, which would lead to erroneous release rate estimates especially during and after strong release activity (Sakaba and Neher, 2001a), we used 100 μM CTZ (to block desensitization) and 2 mM γ-DGG, a rapid off-antagonist at AMPA receptors. Kynurenic acid could not be used, because we found that it strongly absorbed light below 370 nm wavelength, thus impeding Ca^{2+} uncaging and fluorescence excitation at the shorter wavelength used here (350 nm).

We derived the transmitter release rates by deconvolution of EPSCs with previously described analysis routines written in Igor Pro (Neher and Sakaba, 2001; Sakaba and Neher, 2001a), using EPSC traces that were off-line corrected for the remaining R_S errors (see above). The deconvolution procedure assumes that individual quanta add linearly to produce the measured EPSC. Because miniature EPSCs (mEPSCs) in the presence of CTZ show a clearly double-exponential decay (Schneggenburger and Neher, 2000), deconvolution was done assuming a double-exponential mEPSC decay (Schneggenburger and Neher, 2000; Neher and Sakaba, 2001). The mEPSC amplitude was assumed to be 15 pA for all cells, because mEPSCs in the presence of 100 μM CTZ have an average amplitude of ~30 pA across many cells (Scheuss et al., 2002), and 2 mM γ-DGG reduced EPSCs by ~50% in the presence of 100 μM CTZ (see Fig. 2). An initial guess of the time constants of mEPSC decay to be used in EPSC deconvolution was obtained from a double-exponential fit to the decay of small EPSCs (1–2 nA) evoked by brief presynaptic depolarizations. Deconvolution was then done by further constraining the parameters for the mEPSC decay and by finding the parameters for a simple model of glutamate diffusion (Neher and Sakaba, 2001), which calculates a "residual" current caused by glutamate spillover (for an example of a residual current, see Fig. 3*B*, dotted trace). The parameters were found by reiterative deconvolution of EPSC responses to "fitting protocols"; these are presynaptic depolarizations with different lengths applied at 20–50 ms intervals (Neher and Sakaba, 2001, their Fig. 12). The criteria for an optimal parameter set were as follows: (1) the calculated residual current should, at no time point of the analyzed trace (~500 ms), be larger than the measured EPSC current, (2) negative release rates should not occur and, (3) at times after stimulation when voltage-clamp conditions in the presynaptic terminal were such that no transmitter release is expected, the transmitter release obtained by EPSC deconvolution should be close to 0. After finding the parameters in this procedure, all subsequent traces of a given experiment were deconvolved with the same parameter set.

EPSC deconvolution yielded time course of release rates, and when integrated, of cumulative release. The integrated release rate traces were not further corrected for an assumed refilling process of the RRP. The peak release rate was read out manually from the release-rate trace. The peak release rate of the slow component was approximated as illustrated in Figure 3*C* (right), by fitting the second, slower decay phase with a line and back-extrapolating to 2.5 times the decay time constant of the fast release component.

To quantify the kinetics of transmitter release, the integrated release rate traces obtained from EPSC deconvolution were fitted within the first 100 ms after stimulation by several functions: line, one-exponential, one-exponential + line, two-exponential, two-exponential + line, and three-exponential. The validity of these fits was checked taking the following

constraints into account: (1) onset of release in the fitted function must not start before stimulation, (2) the time constants of all components of a multiexponential function (i.e., two-exponential, two-exponential + line, and three-exponential) must differ by more than threefold, (3) each exponential amplitude must contribute by at least 10%, (4) the linear component, if part of the fitting function, must have a positive slope, (5) the maximum of the residual (difference trace between fitted data and fit function) must be smaller than 100 vesicles, and (6) the integrated residual had to be smaller than two vesicles within the fitting range of 100 ms. Among those fits that were accepted as valid, the best fit was determined by the following order, with preference for simplicity: (1) line, (2) one-exponential + line, (3) two-exponential + line, (4) one-exponential, (5) two-exponential, and (6) three-exponential. For the plots of release kinetics versus $[Ca^{2+}]_i$ (see Fig. 6*A–D*), the parameters from the best fit only were displayed. For short presynaptic depolarizing stimuli (see Fig. 7), the fast component of release was approximated by the number of vesicles released within the first 2 ms after the onset of release.

Model calculations. For the simulations (see Fig. 6), we implemented two different models. First, a "one-pool model" was implemented that assumes that all vesicles in the readily releasable pool ($n = 1500$) have the same Ca^{2+} sensitivity. After depletion, there was a simple refilling step from an unlimited reserve pool (see Fig. 6*G*), with maximal speed of two vesicles per millisecond. Ca^{2+}-dependent release was modeled according to an allosteric model of Ca^{2+} binding and vesicle fusion (see Fig. 6*G*) (Lou et al., 2005). The differential equations for this reaction scheme were solved numerically with an Euler approach (step size, 1 μs) written in Igor Pro (WaveMetrics). For each Ca^{2+} waveform (see below), the model calculated the accumulation of vesicles into the fused state (see Fig. 6*E*,*F*, bottom row), which is equivalent to integrated release rate traces. These traces were subsequently analyzed by the same series of multiexponential fits as used for the analysis of experimental data (see above). The resulting estimates of time constants, peak release rates, and number of released vesicles (as obtained by the amplitude of exponential fits) are shown superimposed in Figure 6*A–D* (color symbols connected by lines). Similar to the data, the best fit function depended on $[Ca^{2+}]$. Parameters obtained from single-exponential fits are shown by round symbols, whereas parameters obtained from double-exponential or double-exponential + line fits are shown by open triangles (see Fig. 6*A–D*). In the case of the one-pool model, parameters for the allosteric model of Ca^{2+} binding and vesicle fusion (see Fig. 6*G*) were as follows: $k_{on} = 1.4 \times 10^8\ M^{-1}\ s^{-1}$; $k_{off} = 4000\ s^{-1}$; $b = 0.5$; $l_+ = 2 \times 10^{-4}\ s^{-1}$; $f = 31.3$.

For the "two-pool model," we assumed two parallel pools of readily releasable vesicles with different apparent Ca^{2+} sensitivity. The FRP had 1500 RRP vesicles with an allosteric Ca^{2+} sensor, with the same parameters as used for the one-pool model (see above). The slowly releasable subpool (SRP) had 1300 vesicles with an allosteric Ca^{2+} sensor with a reduced fusion willingness ($l_+ = 7 \times 10^{-6}\ s^{-1}$). The parameters of Ca^{2+} binding (k_{on}, k_{off}, and b) were the same as for the FRP.

The kinetic schemes were driven by Ca^{2+} waveforms that aimed at realistically representing the time course of $[Ca^{2+}]_i$ during flash photolysis (see Fig. 6*E*,*F*, top row). Thus, the rise of the $[Ca^{2+}]_i$ time course was simulated separately using the measured time course of the flash-lamp discharge (see above), as described previously (Schneggenburger and Neher, 2000). The resulting $[Ca^{2+}]_i$ time course followed a ramp-like initial phase reaching peak within 0.6 ms (Fig. 6*E*,*F*, inset). In one group of simulations, $[Ca^{2+}]_i$ stayed constant (Fig. 6*E*,*F*, blue and red traces), whereas in another series of simulations, $[Ca^{2+}]_i$ decayed linearly down to 50% of its peak value after 100 ms (Fig. 6*E*,*F*, green and yellow dotted traces), a similar rate of decay as observed experimentally (see Results). In both cases, we accounted for a possible spatial variability of peak $[Ca^{2+}]_i$ values (Fig. 1). This was done by simulating, for each $[Ca^{2+}]_i$, vesicle fusion for $n = 15$ $[Ca^{2+}]_i$ waveforms with peak values in the range of 0.8- to 1.2-fold of the simulated mean $[Ca^{2+}]_i$. The cumulative release traces shown in Figure 6, *E* and *F* (bottom row), are mean traces, weighted before averaging according to the distribution of peak $[Ca^{2+}]_i$. The assumed distribution was Gaussian, with a coefficient of variation of 0.07, as observed experimentally (Fig. 1). These simulations were repeated for $n = 8$ mean $[Ca^{2+}]_i$ in the range of 2.4–50 μM.

Average data are reported as mean ± SEM if not stated otherwise, and statistical significance was assessed by Student's *t* tests.

Results

Combined presynaptic capacitance measurements and EPSC deconvolution

Previous work at the calyx of Held has shown that prolonged presynaptic voltage-clamp depolarizations (30–50 ms length) lead to a fast and a slow component of transmitter release, as analyzed by EPSC deconvolution (Sakaba and Neher, 2001a,b). This might indicate that readily releasable vesicles at the calyx of Held can be divided into a fast and a more slowly releasable (sub)pool of RRP vesicles (Sakaba and Neher, 2001b) (for review, see Matthews, 2001; Schneggenburger et al., 2002). With presynaptic membrane capacitance measurements, however, a fast and a slow component of release from the RRP have not been distinguished (Sun and Wu, 2001). To address this discrepancy and also to verify the deconvolution approach, we combined simultaneous measurements of EPSCs and of presynaptic membrane capacitance. Because capacitance cannot be measured during a depolarizing step, we tracked the release time course by applying presynaptic voltage-clamp depolarizations of different lengths and measured the capacitance jump after each depolarization (Horrigan and Bookman, 1994; Sun and Wu, 2001; Kushmerick et al., 2006). The EPSCs were recorded simultaneously, in the presence of CTZ (100 μM) and, subsequently, in the presence of CTZ plus 2 mM of the AMPA-receptor antagonist γ-DGG (Fig. 2*A*, black and red traces, respectively).

In Figure 2*A*, presynaptic Ca^{2+} currents (*A1*), postsynaptic EPSCs (*A2*), and release rates as well as integrated release rate traces (*A3*, dotted, and continuous traces, respectively) are shown. Increasing the lengths of the depolarizations initially led to an increase in the EPSC amplitude. With presynaptic depolarizations longer than ~4 ms, the EPSC amplitude stayed constant at a maximal value, but the decay of the EPSCs became increasingly slower (Fig. 2*A2*, see EPSCs from the shorter depolarizations superimposed over the EPSC evoked by the 64 ms depolarization). The slowed decay of the EPSCs indicates transmitter release that occurs after the peak of the EPSCs. To quantify the amount of release, we applied EPSC deconvolution (Neher and Sakaba, 2001) and integrated the resulting release rate traces to obtain a measure of cumulative release (Fig. 2*A3*, continuous traces). The integrated release rate trace in response to the longest depolarization (64 ms) is also shown in Figure 2*C*. It was best fitted with a double-exponential + line function, with fast and slow time constants of 1.7 and 19 ms. On average, the time constants were 3.6 ± 0.7 and 47 ± 14 ms, with an estimated number of 1131 ± 210 and 2506 ± 1069 vesicles released in the fast and the slow component, respectively ($n = 4$ cells).

In Figure 2*B*, the presynaptic membrane capacitance traces are shown. The capacitance jumps were analyzed in brief (30 ms) time windows at 100 ms after the depolarizations (Fig. 2*B*, pink and gray bars). In Figure 2*D*, the capacitance jumps (filled symbols, right axis) and the cumulative release at the end of the depolarizations as estimated by EPSC deconvolution (open symbols, left axis) are superimposed. Both methods reveal a rapid release component within the first 4 ms, followed by a slower release phase that, after another ~60 ms, had released an approximately equal amount of vesicles as released during the fast component.

To average the data, the cumulative release estimates from deconvolution and capacitance jumps were normalized to their respective values for 8 ms depolarizations and averaged ($n = 4$

cells) (Fig. 2*E*). Inspection of the capacitance data in Figure 2*E* (filled symbols) shows that the capacitance jump evoked by 16 ms depolarizations was larger than the one evoked by 8 ms steps ($p = 0.05$), and the relative capacitance jumps for depolarizations of 32 and 64 ms lengths were significantly larger than the ones evoked by 8 ms depolarizations ($p < 0.01$). This suggests that significant additional release took place with depolarizing steps longer than 8 ms. In previous work, a slow release component at times >10 ms was not observed in capacitance measurements at the calyx (Sun and Wu, 2001) (but see Kushmerick et al., 2006). The time course of cumulative release estimated by the capacitance jumps and by EPSC deconvolution agreed well (Fig. 2*E*), indicating that the results of EPSC deconvolution were not strongly distorted by postsynaptic receptor desensitization or saturation. This conclusion is also confirmed by the finding that application of 2 mM γ-DGG, a low-affinity, rapid-off antagonist of AMPA receptors (Liu et al., 1999; Wadiche and Jahr, 2001; Foster et al., 2002), did not significantly change the release rate estimates. For the depolarizations of 4, 16, and 64 ms lengths (Fig. 2*A3*, compare black and red dotted traces), the peak release rates were 107 ± 30, 103 ± 21, and 82 ± 14% of the control values in the presence of CTZ alone, respectively ($n = 4$ cell pairs). Thus, the experiments of Figure 2 show that the time course of transmitter release estimated by EPSC deconvolution and by presynaptic membrane capacitance measurements agreed reasonably well. Both measurements indicate that, with presynaptic depolarizations >10 ms, a fast and a slow release component occur, in agreement with previous results obtained by EPSC deconvolution (Sakaba and Neher, 2001a,b).

Ca^{2+} uncaging induces a fast and a slow component of transmitter release

To investigate whether fast and slow transmitter release is caused by a mechanism intrinsic to the vesicle fusion machinery, such as, for example, a difference in the Ca^{2+} sensitivity of vesicle fusion between RRP vesicles, we evoked transmitter release by Ca^{2+} uncaging. Because Ca^{2+} uncaging produced spatially homogenous elevations of $[Ca^{2+}]_i$ as revealed by Ca^{2+} imaging (Fig. 1) (see Materials and Methods), the appearance of two kinetically distinct release components would indicate that intrinsic mechanisms are responsible for the differences in release kinetics.

In the type of experiment illustrated in

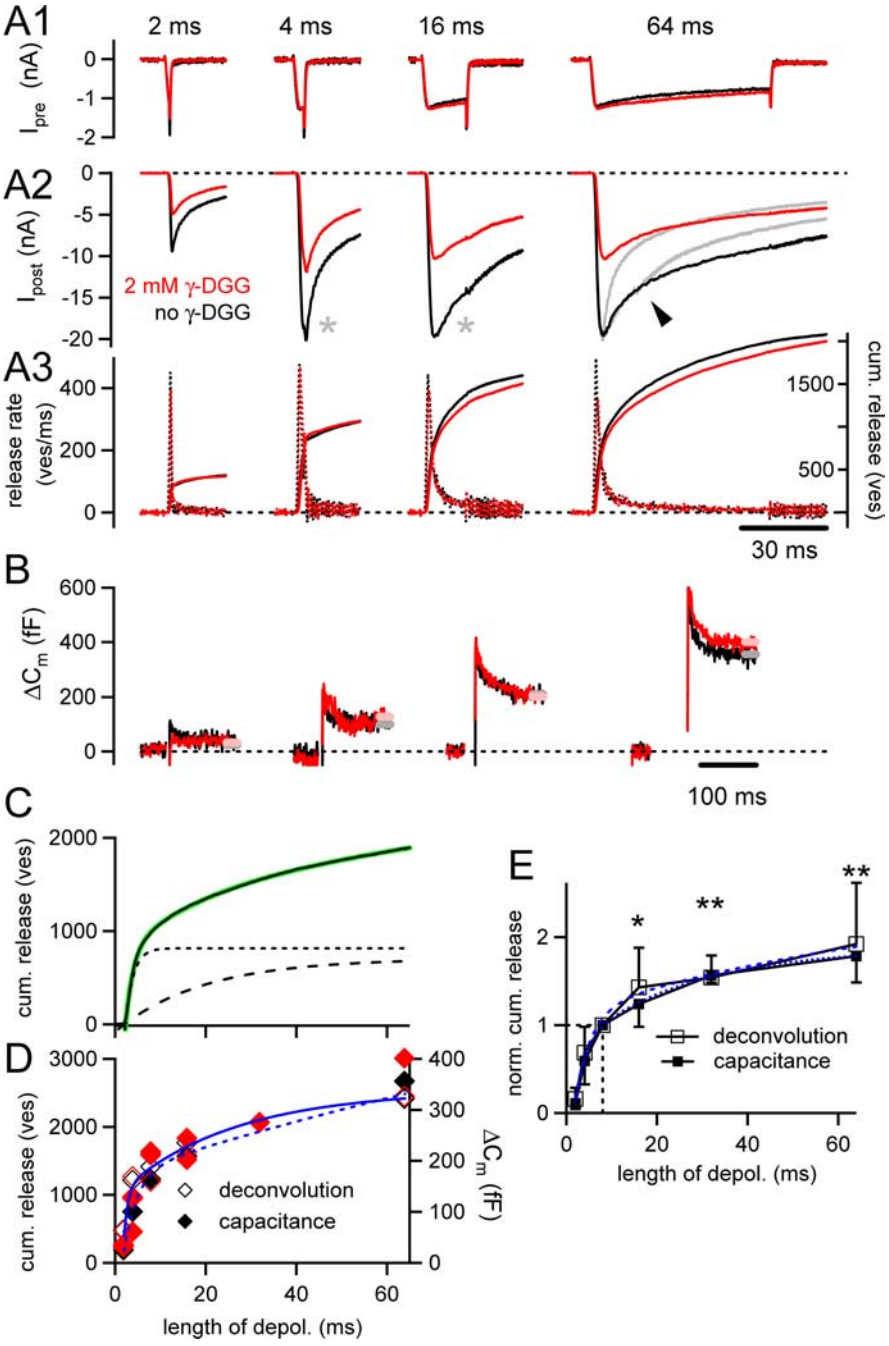

Figure 2. EPSC deconvolution and presynaptic membrane capacitance both report a fast and a slow component of transmitter release. ***A1***, Presynaptic Ca^{2+} currents. ***A2***, EPSCs. ***A3***, Transmitter release rates (dotted traces) and integrated release rates (continuous traces for a series of presynaptic depolarizations to 0 mV of different lengths). The experiment was first done in the presence of CTZ (black traces) and subsequently in the additional presence of 2 mM γ-DGG (red traces). The EPSCs in response to 4 and 16 ms depolarizations are also superimposed onto the EPSC evoked by a 64 ms depolarization (see asterisks and gray traces in ***A2***). Note the slowing of the EPSC decay when longer presynaptic depolarizations were applied (see arrowhead in ***A2***). ***B***, Presynaptic membrane capacitance traces, for the same experiment as shown in ***A***. The superimposed pink and gray bars indicate the time windows (30 ms) during which the poststimulus capacitance values were measured. ***C***, Integrated release rate trace as obtained by EPSC deconvolution in response to a 64 ms depolarization. The trace was fitted by a double-exponential + line function (see green fit line), and the fast- and slow components of the fit are drawn separately (dotted and dashed line, respectively). ***D***, Plot of the capacitance jumps (filled symbols) and cumulative transmitter release from EPSC deconvolution (open symbols) as a function of the length of the depolarization, in the absence (black symbols) or presence (red symbols) of 2 mM γ-DGG. This is the same cell as shown in ***A***. Note that both the capacitance jumps and the cumulative release obtained from EPSC deconvolution indicate a fast and a slow component of release. Both datasets were fitted with double-exponential functions (continuous line, deconvolution; dotted line, capacitance). ***E***, Average cumulative release normalized to the value at 8 ms ($n = 4$ cells). The capacitance jumps for the 32 and 64 ms depolarizations were significantly larger than the ones evoked by the 8 ms depolarization. (**$p < 0.01$), whereas the difference between 16 and 8 ms depolarizations was less significant (*$p = 0.05$).

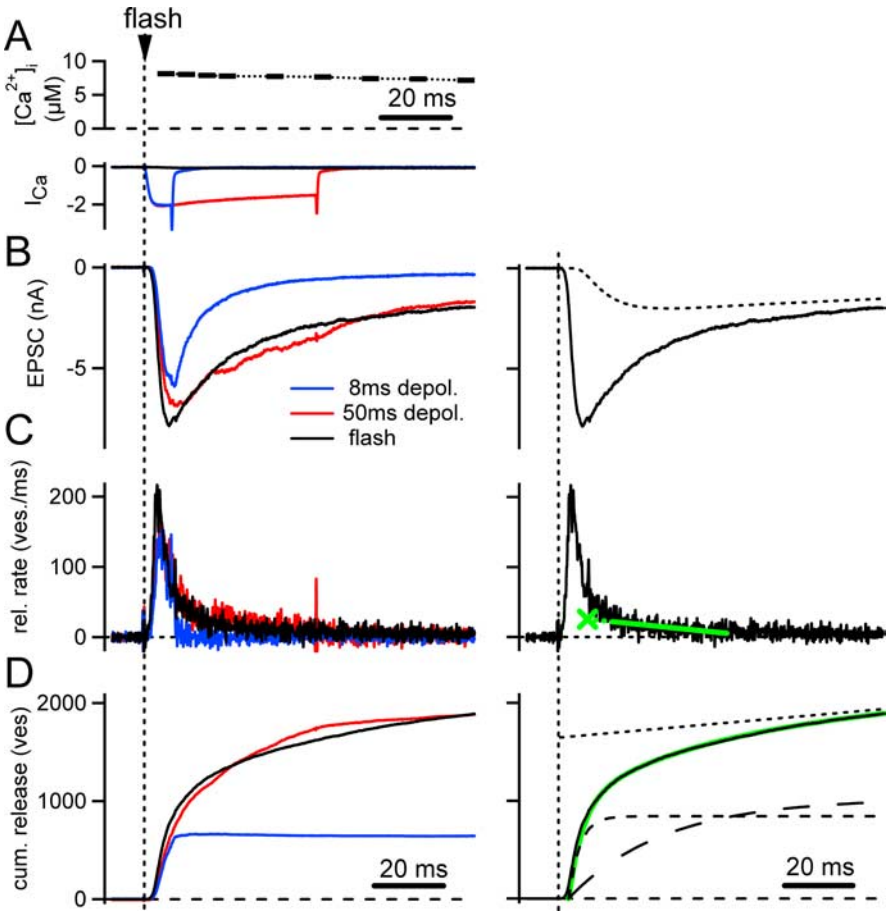

Figure 3. Presynaptic Ca^{2+} uncaging evokes a fast and a slow release component similar as long presynaptic depolarizations. ***A***, Three different Ca^{2+} stimuli were applied in the same presynaptic terminal: a Ca^{2+}-uncaging stimulus that elevated $[Ca^{2+}]_i$ to 8 μM (black traces) and a short (8 ms) and a long (50 ms) presynaptic depolarization to 0 mV (blue and red traces, respectively). ***B***, EPSCs induced by the presynaptic stimuli shown in ***A***, with identical color code. In the right, the flash-evoked EPSC is shown, together with the spillover current estimated during the EPSC deconvolution analysis (see Materials and Methods). ***C***, Release rates resulting from the deconvolution of the EPSCs shown in ***B***. In the right, the release rate in response to the flash is shown again, together with a line fit (green line) that was used to extrapolate the peak release rate of the slow component (see Materials and Methods). ***D***, Integrated release rate traces. The cumulative release rate trace obtained after Ca^{2+} uncaging (black trace) was fitted with a double-exponential function (right, green fit line underlying the data trace), giving fast and slow time constants (and amplitudes) of 3.2 ms (812 vesicles) and 28 ms (994 vesicles). The fast and slow exponential components of the fits are drawn separately (dashed black lines, right). The linear component of the fit is displayed as well (dotted line). Note the similarity of the cumulative release for the Ca^{2+}-uncaging stimulus and for the long depolarization (black and red trace, respectively; left).

Figure 3, we aimed to directly compare transmitter release evoked by Ca^{2+} uncaging and by short and long presynaptic voltage-clamp depolarizations. To do so, we used a low concentration of DM-nitrophen (1 mM) highly loaded with Ca^{2+} (0.85 mM $CaCl_2$; see Materials and Methods) to minimize any interference of the (free) Ca^{2+} buffer DM-nitrophen with depolarization-evoked release. In the cell shown in Figure 3, a flash was applied that elevated $[Ca^{2+}]_i$ to ~8 μM. This Ca^{2+}-uncaging stimulus evoked a rapidly rising (20–80% rise time, 2.0 ms) EPSC of 8 nA amplitude (Fig. 3*B*, black trace) that decayed slowly, with fast and slow time constants of 18 and 56 ms in a double-exponential fit. In the same cell, we also evoked release by a short (8 ms) and a long (50 ms) depolarization to 0 mV (Fig. 3, blue and red traces, respectively), aiming to selectively release the fast and the fast and slow release components (Fig. 2). Both depolarizations evoked rapidly rising EPSCs, and, as expected, the EPSC evoked by the long depolarization decayed slowly (Fig. 3*B*, blue and red trace, respectively). Interestingly, the EPSC in response to the long depolarization was quite similar to the EPSC evoked by Ca^{2+} uncaging (Fig. 3*B*, red and black traces), suggesting similar underlying transmitter release rates.

The transmitter release rates resulting from deconvolution of the EPSCs (Fig. 3*C*) and the integrated release rate traces (Fig. 3*D*) also indicated that transmitter release evoked by the flash and by the long depolarization were similar and consisted of several kinetic phases (Fig. 3*D*, red and black trace). The cumulative release in response to the short depolarization, conversely, stopped at the end of the presynaptic depolarization and, as expected, overlaid well with the fastest phase of cumulative release evoked by the long depolarization (Fig. 3*D*, blue trace).

The experiment in Figure 3 suggests that presynaptic Ca^{2+} uncaging induces transmitter release that, similar as the response to long depolarizations, occurs in more than one kinetic component. To analyze the various kinetics components of transmitter release, the integrated release rate traces were fitted with various single- or double-exponential functions with or without an additional linear component (for details, see Materials and Methods). For the Ca^{2+}-uncaging-evoked EPSC shown in Figure 3, a double-exponential + line function fitted the data best (Fig. 3*D*, right, green fit line), with fast and slow time constants of 4 and 32 ms, respectively, and a late linear rise of three vesicles per millisecond. It is likely that the fast and the slow component reflect two kinetic components of release from the RRP, whereas the late, linearly rising component, with a slope of 2.2 ± 0.6 ms ($n = 15$) for Ca^{2+}-uncaging stimuli between 8 and 15 μM $[Ca^{2+}]_i$, reflects a slower process of RRP refilling. For Ca^{2+}-uncaging stimuli that raised $[Ca^{2+}]_i$ to 10–15 μM, we found that most cumulative release rates ($n = 16$ of 20) were best fitted with double-exponential + line functions, with average fast and slow release time constants of 1.9 ± 0.3 and 44 ± 11 ms, respectively (see also Fig. 6*A*, red average symbols).

The number of vesicles released in the fast kinetic component increases with Ca^{2+}

We next wished to investigate whether biphasic transmitter release kinetics in response to Ca^{2+} uncaging occurred over a wider range of $[Ca^{2+}]_i$, by applying Ca^{2+}-uncaging stimuli with different light intensities. In the experiment shown in Figure 4, two step-like $[Ca^{2+}]_i$ increases to 5.4 and 7 μM elicited small EPSCs with prolonged rise times (Fig. 4*B*, black and green traces, respectively). Higher Ca^{2+} steps evoked larger EPSCs, which rose more rapidly (Fig. 4*B*, blue and red traces), in agreement with previous findings (Bollmann et al., 2000; Schneggenburger and Neher, 2000). Deconvolution of the EPSCs gave the release rate traces shown in Figure 4*C*. We again integrated the release rate traces (Fig. 4*D*) and applied the exponential fitting routines to the resulting cumulative release traces. These were best fitted by

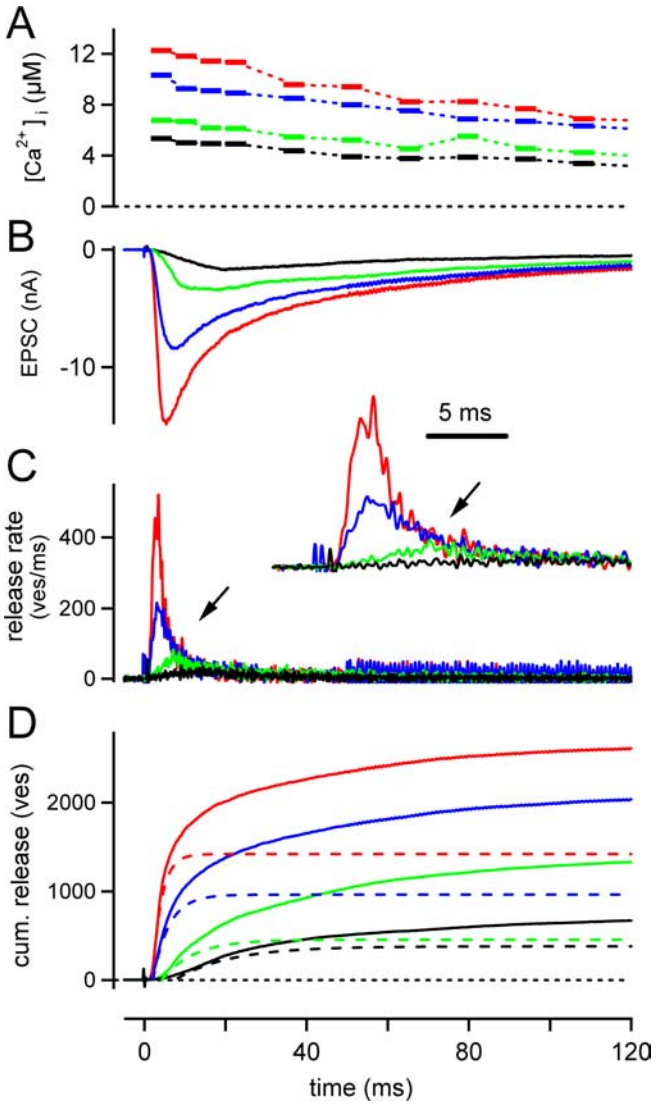

Figure 4. Submaximal release of fast releasable vesicles. ***A***, Ca^{2+}-uncaging stimuli of different intensities produced a series of presynaptic $[Ca^{2+}]_i$ elevations. ***B***, EPSCs. ***C***, Transmitter release rates. ***D***, Cumulative release, all in response to the $[Ca^{2+}]_i$ elevations shown in ***A***. Traces with matched colors refer to the same flash. The integrated release rate traces (***D***) were fitted with double-exponential or double-exponential + line functions, and the fast exponential components of these fits are shown (dashed lines). Note that Ca^{2+} steps of increasing amplitudes lead to a marked increase of the fast release component.

double-exponential (in the case of the black and the blue trace) or by double-exponential + line (green and red trace) functions. The fast exponential components of these fits are shown by dashed lines in Figure 4*D*. Surprisingly, the amplitude of the fast component markedly increased with $[Ca^{2+}]_i$ steps of increasing amplitudes (Fig. 4*D*, dashed traces). Thus, for the four $[Ca^{2+}]_i$ steps applied in the example of Figure 4, the estimated number of vesicles released during the fast release component was only ~300 for the smallest $[Ca^{2+}]_i$ step but ~1500 for a $[Ca^{2+}]_i$ step to 12.7 μM.

The increased fast release component is also apparent in the release rates traces (Fig. 4*C*). $[Ca^{2+}]_i$ steps of increasing amplitudes led to increased peak transmitter release rates, but, during the decaying phase of transmitter release at times longer than ~5 ms after the flash, the various release rate traces superimposed quite well (Fig. 4*C*, arrow and inset). As a consequence, the area below the peaks of the transmitter release rate traces was larger for Ca^{2+} stimuli of higher amplitudes, again indicating an increase in the number of fast-released vesicles. We will call this finding submaximal release of fast-releasable vesicles, because Ca^{2+} steps of smaller amplitudes lead to the release of fewer vesicles in the fast release component.

As can be seen in Figure 4*A*, the Ca^{2+}-uncaging stimuli applied under standard conditions (1 or 1.5 mM DM-nitrophen and ~15% monochromator intensity) (see Materials and Methods) were not ideal step-like responses. Rather, $[Ca^{2+}]_i$ decayed to 78 ± 3% of its peak amplitude at 50 ms after the flash because of Ca^{2+} extrusion. It is possible, therefore, that submaximal release of fast-releasable vesicles was caused by the decay of $[Ca^{2+}]_i$ after the flashes, because the transmitter release rate depends highly supralinearly, with a fourth to fifth order power relationship, on $[Ca^{2+}]_i$ (Bollmann et al., 2000; Schneggenburger and Neher, 2000). Below, we investigate this possibility by simulations (see Fig. 6*E*,*F*). To address this possibility experimentally, we performed an additional set of experiments in which we slowed the $[Ca^{2+}]_i$ decay after flashes by using higher DM-nitrophen concentrations (3 mM) and a higher intensity of monochromator illumination (~60%) (see Materials and Methods). In these experiments (Fig. 5), we also asked whether the number of vesicles released in the fast and the slow component are independent from each other or whether there was a reciprocal relationship.

Figure 5*A* shows an experiment in which Ca^{2+}-uncaging stimuli covered a wide range of $[Ca^{2+}]_i$, and transmitter release evoked by Ca^{2+} uncaging was tracked for a prolonged time by EPSC deconvolution. After 100 ms, a strong presynaptic depolarization to 0 mV was given to deplete the RRP. Under these conditions, presynaptic $[Ca^{2+}]_i$ decayed to 88 ± 5% of its peak value at 50 ms after the flash ($n = 19$ flashes in 10 cells), and, thus, the $[Ca^{2+}]_i$ decay was slower than in the Ca^{2+}-uncaging experiments of Figures 1, 3, and 4 (78 ± 3%) (see above). In the experiment of Figure 5*A*, a small $[Ca^{2+}]_i$ step to 4 μM induced a very slowly rising EPSC of 0.1 nA final amplitude, indicating linearly rising cumulative release (Fig. 5*A2*, bottom black trace). With Ca^{2+} stimuli of 6 μM or higher, EPSCs peaked within ~10 ms after the flash, and the integrated release rate traces showed a fast and a slow component of release, as observed previously (Figs. 3, 4). The number of vesicles released in the fast component, as estimated from the fast component of double-exponential + line fits, markedly increased with $[Ca^{2+}]_i$ steps of increasing amplitudes (Fig. 5*A2*, bottom, dotted lines). Thus, submaximal release of fast-releasable vesicles was again observed.

Surprisingly, these experiments indicated that the number of vesicles released in the fast and the slow release component were differentially regulated by the amplitude of the Ca^{2+} stimuli. In Figure 5*B*, the number of vesicles released in the fast and in the slow release component, as well as the total release, is plotted as a function of $[Ca^{2+}]_i$ for the same cell pair as shown in Figure 5*A*. At low $[Ca^{2+}]_i$, both the fast and the slow release component increased with $[Ca^{2+}]_i$ steps of increasing amplitudes. Above a certain threshold (~7 μM $[Ca^{2+}]_i$ in this cell), however, the fast component continued to increase whereas the slow component decreased (Fig. 5*B*, filled and open squares, respectively). Thus, the fast release component increased on the expense of the slow one, whereas the total amount of release, as measured at the end of the strong presynaptic depolarization, was constant (Fig. 5*B*, round symbols).

An increase of the fast release component on the expense of the slow one with $[Ca^{2+}]_i$ steps of increasing amplitudes was confirmed across all cell pairs measured under these conditions ($n = 9$). In the plot of Figure 5*C*, the amplitude of the fast and the

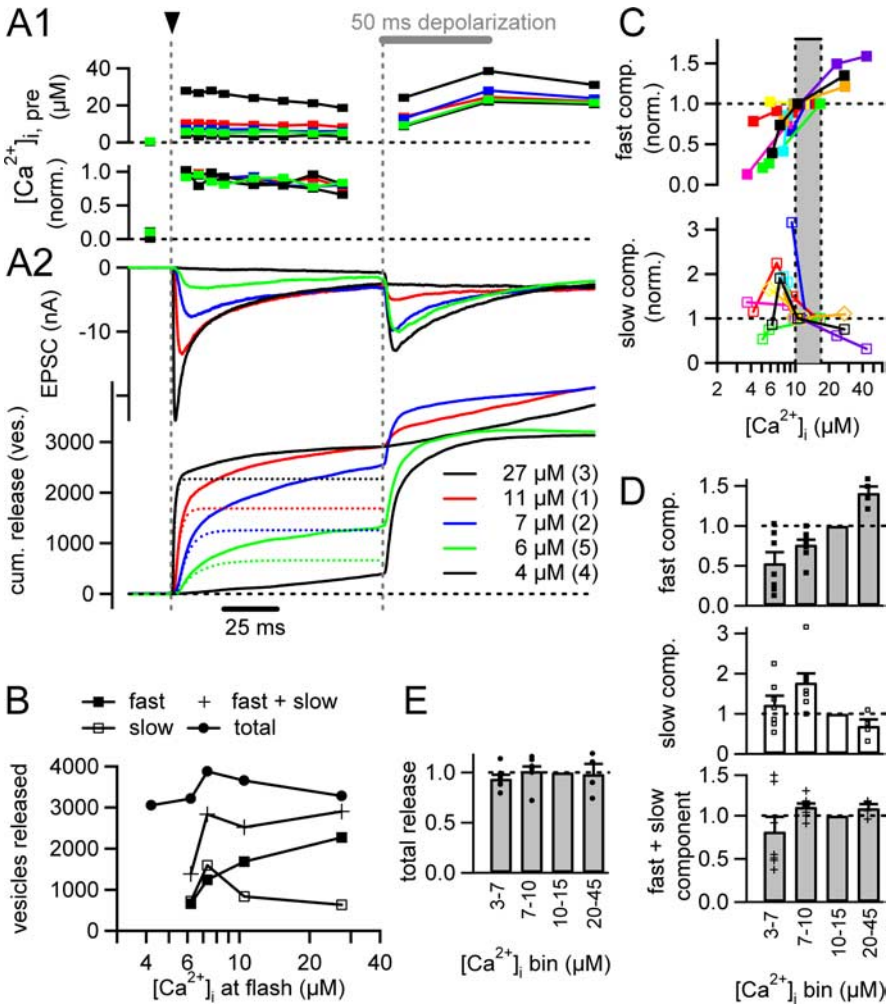

Figure 5. Differential regulation by Ca^{2+} of the number of fast and slowly released vesicles. ***A1***, $[Ca^{2+}]_i$ was increased to different levels by Ca^{2+} uncaging (flash at arrowhead), and this was followed after 100 ms by a 50 ms depolarization to 0 mV (horizontal gray bar). $[Ca^{2+}]_i$ traces are shown in micromolar (top), as well as normalized to their peak values (bottom). Within the first 50 ms, $[Ca^{2+}]_i$ decayed to 88% of its peak value in this cell. ***A2***, The corresponding EPSCs (top) and cumulative release rates (bottom), in the same color code as the traces shown in ***A1***. The dotted lines in the bottom represent the fast components of double-exponential fits to the cumulative release traces. Note that the fast component markedly increased with Ca^{2+} steps of increasing amplitudes. The numbers in brackets indicate the temporal sequence of Ca^{2+}-uncaging stimuli. ***B***, The number of vesicles released in the fast and slow component, as well as the summed release (cross symbols), and the total release after the 50 ms depolarization is plotted as a function of $[Ca^{2+}]_i$, for the same cell pair as shown in ***A***. Note that the number of vesicles released in the fast component (filled squares) increases on the expense of the number of slowly released vesicles (open squares), whereas the total release after the flash and the 50 ms depolarization (round symbols) was nearly constant. ***C***, The amplitude of the fast and slow release components were normalized to their values in a range of 10–15 μM $[Ca^{2+}]_i$ and plotted as a function of $[Ca^{2+}]_i$. Each color represents data from one cell pair ($n = 9$ pairs); black symbols represent the same cell pair as shown in ***A*** and ***B***. The fast component clearly increases with $[Ca^{2+}]_i$ steps of increasing amplitudes, whereas the slow component shows a tendency toward smaller amplitude, more than ~7 μM $[Ca^{2+}]_i$ (top and bottom, respectively). ***D***, The data shown in ***C*** were averaged for the indicated four ranges of $[Ca^{2+}]_i$. This revealed a significant increase of the fast component with $[Ca^{2+}]_i$ (top) and a concomitant decrease of the slow component (middle). The bottom shows the summed release evoked by Ca^{2+} uncaging, obtained by summing the amplitude values of the fast and the slow exponential component. ***E***, Plot of the total release after the 50 ms depolarizations, for the same four binned $[Ca^{2+}]_i$ ranges as shown in ***D***.

slow release components were normalized to the values obtained at 10–15 μM $[Ca^{2+}]_i$ to facilitate a comparison between cells, and the data from each cell are shown in a different color. When the data from the individual cells were averaged in four bins of $[Ca^{2+}]_i$ (3–7, 7–10, 10–15, and 20–45 μM) (Fig. 5*D*), a significant increase of the fast component was apparent (Fig. 5*D*, top) ($p = 0.015$, 0.007, and 0.015 for the lowest, second lowest, and highest $[Ca^{2+}]_i$ bin with respect to the value at 10–15 μM $[Ca^{2+}]_i$; one-sample *t* test), whereas the slow component decreased above 7 μM $[Ca^{2+}]_i$. Nevertheless, the sum of vesicles released in the fast and the slow component, as estimated by the summed amplitude values of the two components, was constant beyond a certain threshold value of $[Ca^{2+}]_i$ (Fig. 5, *D*, bottom, *B*, cross symbols for a single-cell example). Also, the total number of vesicles released after the final, strong presynaptic depolarization was constant (Fig. 5*E*; *B*, round symbols). These findings indicate that release within the exocytotic burst at the calyx of Held draws from a common, limited pool of RRP vesicles. However, the relative contribution of a fast and a slow release component to the exocytotic burst is not fixed but seems to be a function of the $[Ca^{2+}]_i$ reached after the flash.

The Ca^{2+} dependency of fast and slow transmitter release

To summarize the Ca^{2+}-uncaging data, we plotted the release time constants, the release rates, and the number of vesicles released in the fast and the slow release component as a function of $[Ca^{2+}]_i$ (Fig. 6*A–D*) ($n = 104$ flashes in $n = 55$ paired recordings). Above 4 μM $[Ca^{2+}]_i$, the majority of the responses ($n = 66$ of 96) was best fitted by a double-exponential + line function ($n = 63$ of 96) or by double-exponential functions ($n = 3$ of 96), and these responses are represented by filled and open triangles in Figure 6*A–D*, referring to the fast and the slow exponential component, respectively. In a range of 10–15 μM $[Ca^{2+}]_i$, the fast and the slow components had average time constants of 1.9 ± 0.3 and 44 ± 11 ms, respectively (Fig. 6*A*, red average symbols), and 1507 ± 178 and 1319 ± 228 vesicles were released in the fast and the slow release component in this range of $[Ca^{2+}]_i$ (Fig. 6*C*,*D*, red average symbols). In response to weaker Ca^{2+}-uncaging stimuli (2–4 μM $[Ca^{2+}]_i$), we often observed integrated release rate traces that were best fitted by a line (Fig. 6*A*, open squares; for an example, see Fig. 5*A2*, bottom black trace), by a single-exponential (Fig. 6*A*, open circles), or by a single-exponential + line (Fig. 6*A*, open diamonds) function.

As expected from the Ca^{2+} dependency of transmitter release, the time constants of the fast and the slow release components decreased with Ca^{2+} steps of increasing amplitudes, and the release rates of the fast and the slow release components increased with $[Ca^{2+}]_i$ (Fig. 6*A*,*B*). Line fits of the logarithmized datasets indicated slopes of −1.7 for the time constants (Fig. 6*A*, red and pink fit lines) in the range of 4–15 μM $[Ca^{2+}]_i$ and slopes of 2.5 and 0.9 for the peak release rates of the fast and the slow component, respectively (Fig. 6*B*, red and pink fit lines).

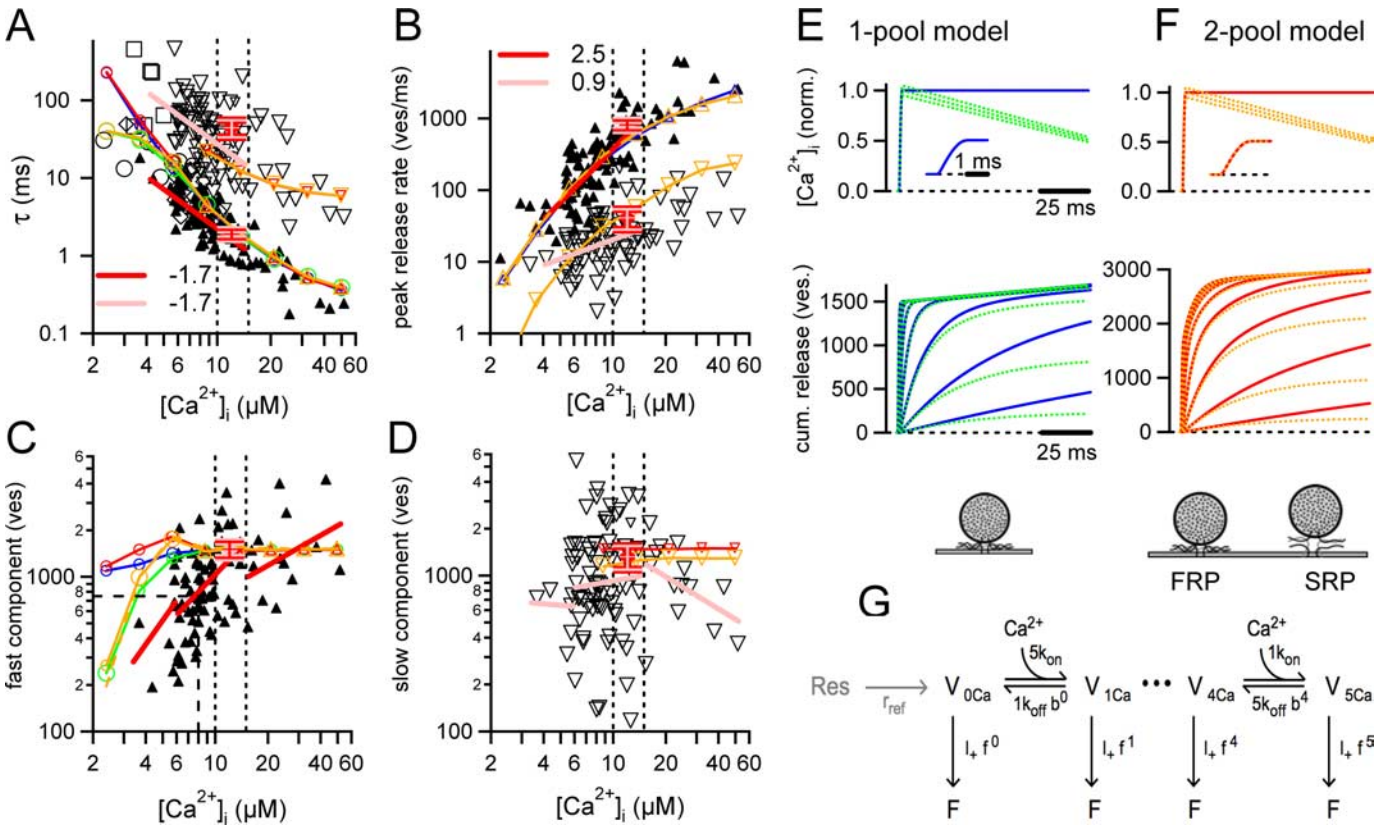

Figure 6. Intracellular Ca^{2+} dependence of the fast and the slow component of transmitter release. Time constants of release (***A***), peak release rates (***B***), and amplitudes of the fast (***C***) and the slow (***D***) component of release are plotted against the amplitude of the $[Ca^{2+}]_i$ steps produced by Ca^{2+} uncaging. ***A*** shows the time constants estimated from the exponential fit analysis, in which various combinations of exponential and line functions were fitted to integrated release rate traces (see Materials and Methods). Each black symbol is chosen according to the fit function that described the data best (open squares, line; open circles, single exponential; open diamonds, single exponential + line). Note that, above ~4 μM $[Ca^{2+}]_i$, most cumulative release traces were best fitted by double-exponential or double-exponential + line functions, and the corresponding parameters obtained from the fast and the slow exponential component are shown as filled and open triangles, respectively. In ***A–D***, the logarithmized datasets were fitted with line functions (see red and pink lines), giving slope values as indicated. The data in the range of 10–15 μM $[Ca^{2+}]_i$ are shown additionally as red average data points. The predictions of the models shown in ***E*** and ***F*** are also shown (symbols connected by lines, in colors). Predictions obtained from single-exponential fits of the simulated release traces are shown by open circles, and those obtained by double-exponential and double-exponential + line fits are shown by triangles. ***E***, ***F***, $[Ca^{2+}]_i$ waveforms (top) used for the model calculations of the cumulative release rates (bottom), according to a one-pool model (***E***) or a two-pool model (***F***). ***G***, The allosteric model of Ca^{2+} binding and vesicle fusion used for the simulations. The state "F" represents the fused state. For the parameter set and for details on the simulations, see Materials and Methods.

The number of vesicles released in the fast release component increased with $[Ca^{2+}]_i$ steps of increasing amplitudes (Fig. 6*C*), again indicating submaximal release of the fast releasable vesicles with $[Ca^{2+}]_i$ steps of lower amplitudes (Figs. 4, 5). An increase in the number of vesicles released in the fast component is also indicated by line fits to selected $[Ca^{2+}]_i$ ranges (3–6, 6–15, and 15–52 μM) (Fig. 6*C*, red fit lines), which show clear positive slopes. The number of slowly released vesicles varied strongly with Ca^{2+}-uncaging stimuli up to ~15 μM, and showed a tendency to decrease with $[Ca^{2+}]_i$ steps >15 μM (Fig. 6*D*, pink fit lines).

Modeling biphasic release with a two-pool model

Our observation that $[Ca^{2+}]_i$ steps by Ca^{2+} uncaging evoked a clearly biphasic transmitter release response over a wide range of $[Ca^{2+}]_i$ (~4 μM up to 50 μM investigated here) (Fig. 6*A–D*) indicates that a mechanism intrinsic to the vesicle fusion machinery causes fast and slow transmitter release, such as, for example, two (sub)pools of readily releasable vesicles with distinct intrinsic release kinetics. On the other hand, our observation of submaximal release is unexpected for readily releasable pool concepts with fixed sizes (Voets, 2000). To test these predictions more stringently and to verify our conclusions, we made model simulations, taking into account a possible spatial variability of the $[Ca^{2+}]_i$ increase produced by Ca^{2+} uncaging (see Materials and Methods) (Fig. 1) and also taking into account the measured decay of $[Ca^{2+}]_i$ after flashes.

We first wanted to exclude the possibility that biphasic release could have been produced by a spatially heterogeneous Ca^{2+}-uncaging signal, acting on an intrinsically homogenous pool of readily releasable vesicles. To do so, we modeled release according to a homogeneous pool of RRP vesicles with a single type of "allosteric" Ca^{2+} sensor (Lou et al., 2005) and an additional replenishment step of two vesicles per millisecond (one-pool model) (for details of model parameters, see Materials and Methods). Release from such a one-pool model was driven by $[Ca^{2+}]_i$ signals that either stayed constant or decayed to 50% after 100 ms (Fig. 6*E*, blue and dotted green traces, respectively). The measured variability of peak $[Ca^{2+}]_i$ values produced by Ca^{2+} uncaging (c.v. of 0.07) (Fig. 1) was built into all simulations (see Materials and Methods). The cumulative release traces resulting from these simulations (Fig. 6*E*, bottom) were best fitted by single-exponential + line functions, regardless of whether the $[Ca^{2+}]_i$ waveforms used for the simulations were constant (Fig. 6*E*, blue traces) or decayed after reaching their peak (Fig. 6*E*, green dotted traces). Thus, the one-pool model predicted a single

release component (Fig. 6*A*, green circles connected by lines), despite taking into account the spatial heterogeneity in the post-flash $[Ca^{2+}]_i$ signal. Because, however, we observed clearly biphasic transmitter release after flashes (Figs. 3–5, 6*A–D*), a mechanism in which all RRP vesicles have the same Ca^{2+} sensitivity of vesicle fusion seems unlikely.

To explain the biphasic release kinetics after Ca^{2+} uncaging, we next analyzed the data with a model that assumes that two populations of RRP vesicles exist with different Ca^{2+} sensitivities (two-pool model) (Fig. 6*F*). Exocytosis speed is intrinsically different for each subpool, and the subpools will be called FRP and SRP for fast and slowly releasable vesicles, respectively. FRP and SRP vesicles might represent different states of maturation of RRP vesicles as found in chromaffin cells (Sorensen, 2004). However, a transition between FRP and SRP was not considered here because release rates occurring within 50 ms or less are the most relevant, a time interval that is probably too short to allow for a significant transition between the subpools. Nevertheless, a replenishment rate of two vesicles per millisecond was implemented for both the SRP and the FRP.

The two-pool model predicted many essential features of transmitter release evoked by Ca^{2+} uncaging. Thus, the model predicted biphasic release kinetics for $[Ca^{2+}]_i$ stimuli above ~6 μM $[Ca^{2+}]_i$, similar as observed (Fig. 6*A*, red and yellow symbols connected by lines). It also predicted quite accurately the Ca^{2+} dependencies of the fast and the slow release time constants (Fig. 6*A*), as well as the peak release rates for the fast and the slow release component (Fig. 6*B*, yellow triangles connected by lines). In the model, release from the FRP was described by a parameter set of the allosteric model of Ca^{2+} binding (k_{on}, k_{off}, and vesicle fusion rate l_+) similar to the one used previously to model peak release rates (Lou et al., 2005). To simulate release of SRP vesicles, we assumed that the vesicle fusion rate l_+ was reduced by a factor of 33, with all other parameters unchanged (for details, see Materials and Methods). The analysis of the data with simulations of a one-pool and a two-pool model thus confirms that release at the calyx of Held must be intrinsically biphasic.

Although the two-pool model predicted the Ca^{2+} dependencies of the fast and the slow release time constants and the peak release rates sufficiently well (Fig. 6*A*,*B*), the model did not quantitatively account for submaximal release, i.e., the finding that the number of fast-released vesicles increased with $[Ca^{2+}]_i$ steps of increasing amplitudes (Fig. 6*C*). The model predicts that a nearly constant number of vesicles is released in the fast release component (Fig. 6*C*, open red circles connected by line). This is expected, because release from a (sub)pool of RRP vesicles with a fixed size should eventually lead to the depletion of the entire (sub)pool, even with small Ca^{2+} steps (Voets, 2000). The data, however, show a clear increase of the number of vesicles released in the fast component in the range of 4–10 μM $[Ca^{2+}]_i$ (Fig. 6*C*).

When we accounted for the measured decay of $[Ca^{2+}]_i$ after flashes, by driving the two-pool model with decaying $[Ca^{2+}]$ steps (Fig. 6*F*, dotted yellow traces), a smaller fast release component resulted for the two lowest simulated $[Ca^{2+}]_i$ stimuli (2.4 and 3.7 μM) (Fig. 6*C*, open yellow circles connected by line). However, the model still predicted a half-maximal release of the FRP (~750 vesicles) at only 3–4 μM $[Ca^{2+}]_i$, whereas the observed half-maximal depletion of FRP vesicles was at ~8 μM $[Ca^{2+}]_i$ (Fig. 6*C*, dashed black lines). When we assumed an even steeper relationship between transmitter release and $[Ca^{2+}]_i$, by using an allosteric model with six Ca^{2+}-binding sites for the FRP vesicles, the amount of predicted submaximal release was nearly unchanged (Fig. 6*C*, dashed yellow line). Thus, the two-pool model could not account quantitatively for the full amount of submaximal release of fast-releasable vesicles. Also, the two-pool model did not predict the observed decrease above 10 μM $[Ca^{2+}]_i$ of the number of slowly released vesicles (Fig. 6*D*, pink fit line >15 μM $[Ca^{2+}]_i$). These findings indicate that other mechanisms, such as an a posteriori decrease of the Ca^{2+} sensitivity of any given RRP vesicle, might contribute to the observed intrinsic differences in release rates (see Discussion).

Submaximal release during trains of action potential-like stimuli

We finally wanted to investigate the role of fast and slowly releasing vesicles during trains of physiological stimuli. We were especially interested in whether, during train stimulation, submaximal release of fast-releasing vesicles is also apparent. To investigate this, we made simultaneous presynaptic and postsynaptic recordings and applied trains of 20 short presynaptic depolarizations at 100 Hz, followed by a final depleting depolarization (Fig. 7*A1*). The width of all depolarizing pulses in a given 100 Hz train was varied, with the aim to produce trains with various initial release probabilities, *p*. In the example of Figure 7*A1*, trains of 1, 1.5, and 2 ms depolarizations to 0 mV were applied, resulting in trains of EPSCs with small, intermediate, and large first EPSC amplitudes (Fig. 7*A1*, bottom).

Inspection of the raw traces in Figure 7*A1* suggested that the total charge transfer of EPSCs increased with increasing release probability of the individual stimuli, suggesting that submaximal release also occurred with train stimulation. We first analyzed the peak EPSC amplitude for each stimulus in the train (Fig. 7*B1*, top). In the resulting depression curves, an increased first EPSC amplitude and an increased rate of depression was apparent at high release probability, but, from the third EPSC onward, the EPSC amplitudes were similar for all three release probabilities (Fig. 7*B1*, top, arrow). This suggested that the cumulative EPSC amplitudes are higher for trains with high release probability. Indeed, in the plot of cumulative EPSC amplitudes, it is seen that the cumulative EPSC amplitude reached after three to four stimuli was larger for high *p* trains (Fig. 7*B1*, bottom). Also, estimating the RRP size by back-extrapolation of the cumulative EPSC plots to time 0, a method often used for estimating pool sizes (Schneggenburger et al., 1999; Bollmann et al., 2000), gave increasing apparent pool sizes for trains with increasing release probability (Fig. 7*B1*, bottom). Thus, submaximal release was also observed during trains of action potential (AP)-like stimuli, in which it showed up as an apparently smaller pool size during trains at moderate release probability, as estimated by the method of cumulative EPSC amplitudes. Although the Ca^{2+} current showed some inactivation during 100 Hz trains (to ~90% of their initial peak amplitudes) (Fig. 7*A*1, top) (Xu and Wu, 2005), additional simulations with a one-pool model showed that Ca^{2+} current inactivation did not significantly contribute to depression of transmitter release during these high stimulation frequencies, consistent with previous work (Xu and Wu, 2005).

Submaximal release was also apparent when transmitter release rates were analyzed by EPSC deconvolution. Deconvolving the EPSCs showed that, with each presynaptic depolarization, there was a fast release component, visible as a rapid upward surge in the cumulative release rate trace (Fig. 7*A2*), followed by a slower release phase after each stimulus (Sakaba, 2006). At the end of the stimulus trains, the slowly released vesicles contributed to ~30–50% of all released vesicles. To analyze the fast release component coupled to each presynaptic depolarization ("phasic release"), we defined the phasic release component as release oc-

curring within 2 ms after the onset of each depolarizing step. The cumulative fast release analyzed in this way is shown as dotted line in Figure 7*A2*. In Figure 7*B2*, the number of fast released vesicles as well as their cumulative number is plotted against time. The shape of these curves is very similar to the corresponding analysis using peak EPSC amplitudes in the same cell pair (Fig. 7*B1*). Thus, the apparent pool size is significantly increased by increasing the Ca^{2+} influx during each AP-like depolarization. The deconvolution also shows that a significant amount of asynchronous release builds up during train stimulation (Sakaba, 2006).

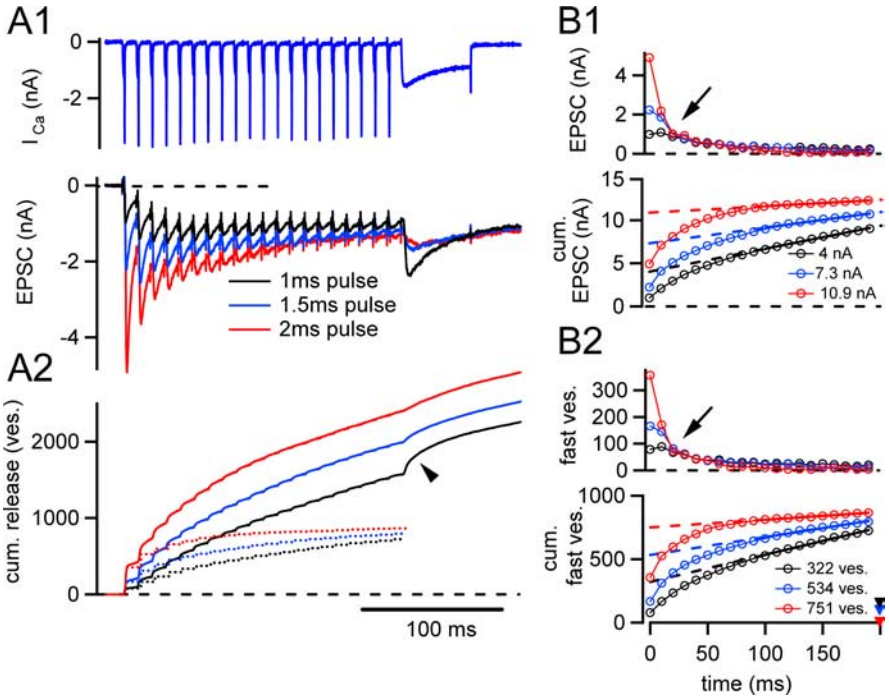

Figure 7. Submaximal release of fast-released vesicles during trains of AP-like depolarizations. ***A1***, Presynaptic Ca^{2+} current (top) and EPSCs (bottom) in response to 100 Hz trains of presynaptic depolarization, followed by a long (50 ms) depolarization to 0 mV. The trains consisted of depolarizations to 0 mV, with durations of 1, 1.5, or 2 ms, aimed at imposing various release probabilities during the trains. ***A2***, Integrated release rate traces for the EPSCs shown in ***A1***. Note that the release response consists of a fast component tightly locked to each presynaptic depolarization, but that, in addition, a slow release component builds up. The cumulative fast release, estimated by analyzing release within 2 ms after each depolarization, is shown by the dotted lines. ***B1***, The EPSC amplitude (top) and the cumulative EPSC amplitude (bottom) are plotted against time during the 100 Hz train (same cell as shown in ***A1***). Note that, despite different first and second EPSC amplitudes, the later EPSC amplitudes converge to similar values for the three different release probabilities (see arrow in the top). As a consequence, the cumulative EPSC amplitude is larger for high release probabilities after a few stimuli. ***B2***, Same analysis as in ***B1*** but now based on the estimated number of vesicles released rapidly (within 2 ms) after each presynaptic depolarization, based on EPSC deconvolution. In the bottom of ***B1*** and ***B2***, the cumulative plots were fitted with lines between the 10th and the 20th stimuli, and the fit lines were back-extrapolated to the beginning of the train. The values for the extrapolated *y*-axis intercept are indicated in each panel. In ***B2***, the estimated number of remaining fast-released vesicles as tested by a final 50 ms depolarization (see ***A2***, arrowhead) is also indicated (filled triangles, bottom).

Discussion

We analyzed the time course of transmitter release under direct control of presynaptic $[Ca^{2+}]_i$ at a large CNS synapse, the calyx of Held. We found that spatially homogeneous $[Ca^{2+}]_i$ steps produced by Ca^{2+} uncaging elicit a fast and a slow component of transmitter release over a wide range of $[Ca^{2+}]_i$. At 10–15 μM $[Ca^{2+}]_i$, the amplitude and the release kinetics of the fast and the slow component are similar to the one observed after prolonged presynaptic voltage-clamp depolarizations (Fig. 2) (see also Sakaba and Neher, 2001b). Thus, our first conclusion is that the fast and slow release produced by prolonged stimuli are primarily caused by a mechanism intrinsic to the vesicle fusion machinery, although additional "positional" differences in the colocalization of RRP vesicles and Ca^{2+} channels remain possible. Detailed analysis of the Ca^{2+}-uncaging data with models that assume (1) a single pool of readily releasable vesicles with homogenous Ca^{2+} sensitivity, and (2) a two-pool model with intrinsically fast and slowly releasable vesicles confirms that a mechanism intrinsic to the vesicle fusion machinery is responsible for fast and slow release, but the simulations also show limitations of classical models with fixed pool sizes. This might indicate that other mechanisms, such as an a posteriori reduction of the Ca^{2+} sensitivity of vesicle fusion after the onset of a prolonged Ca^{2+} stimulus, contribute to the reluctant release of part of the RRP.

Biphasic transmitter release after Ca^{2+} uncaging

The Ca^{2+} dependence of the peak release rates of the fast release component reported here (Fig. 6*B*) is in good agreement with that of previous studies (Schneggenburger and Neher, 2000; Felmy et al., 2003; Lou et al., 2005) (but see Bollmann et al., 2000, who reported a somewhat higher Ca^{2+} sensitivity). We found, by analyzing integrated release rate traces, that Ca^{2+} uncaging evoked a second, slow release phase that, although apparent in some of the previous work (Schneggenburger and Neher, 2000; Felmy et al., 2003; Lou et al., 2005), had not been analyzed before. In combined presynaptic membrane capacitance and EPSC deconvolution measurements (Fig. 2), we verified that the slow release phase reported by EPSC deconvolution was caused by vesicle fusion. In a previous study using Ca^{2+} uncaging and presynaptic capacitance measurements, biphasic secretion kinetics were also found for many responses (Wölfel and Schneggenburger, 2003). A reanalysis of the previous dataset revealed that, in the range of 10–15 μM $[Ca^{2+}]_i$, a majority of capacitance traces (15 of 25) showed biphasic kinetics, with a fast and a slow time constant of 2.8 and 29 ms in the corresponding average capacitance trace (supplemental Fig. 1*A*, available at www.jneurosci.org as supplemental material). These values are in excellent agreement with the time constants obtained by EPSC deconvolution (Fig. 6*A*). Together, our findings leave little doubt that Ca^{2+} uncaging leads to a fast and a slow component of transmitter release at the calyx of Held.

The fast and the slow release component likely represent release of RRP vesicles with different intrinsic release kinetics, but there are two alternative explanations that must be considered. First, biphasic release might be attributable to a spatial heterogeneity in the $[Ca^{2+}]_i$ elevations produced by Ca^{2+} uncaging. The simulations of Figure 6*E* showed, however, that a simple one-pool model with homogeneous Ca^{2+} sensitivity did not predict biphasic release kinetics, even when the measured pixel-to-pixel variability of post-flash $[Ca^{2+}]_i$ (Fig. 1) was taken into account. Thus, possible spatial heterogeneities of $[Ca^{2+}]_i$ after Ca^{2+} un-

caging were not the reason for the observed biphasic release. Second, the slow release component might represent a fast phase of RRP recovery. Kushmerick et al. (2006) interpreted the additional rise in membrane capacitance jumps that occurred between steps of 10 and 30 ms lengths as recovery of the RRP, based on the finding by Sun and Wu (2001) who suggested that the RRP is depleted within 10 ms. Here we find that depolarizations longer than 10 ms lead to a clear second component of capacitance increase (Fig. 2), in agreement with the result of Kushmerick et al. (2006). However, we interpret the second component of capacitance increase, which coincides with the second release component estimated by EPSC deconvolution (Fig. 2), as reluctant release of RRP vesicles (Sakaba and Neher, 2001). This interpretation is corroborated by the finding that $[Ca^{2+}]_i$ steps of increasing amplitudes lead to an increased fast release component on the expense of the slow component such that, at >20 μM $[Ca^{2+}]_i$, most RRP vesicles are released fast (time constant, ~1 ms) and little slow release is left (Fig. 5) (supplemental Fig. 1, available at www.jneurosci.org as supplemental material). Also, above 20 μM $[Ca^{2+}]_i$, the remaining slow release component was so fast (time constant, ~10 ms or less) (Fig. 6*A*) that a recovery process seems unlikely as an explanation for the slow release.

What causes reluctant release of RRP vesicles?

It seems, therefore, that fast and slow transmitter release evoked by Ca^{2+} uncaging reflects an intrinsic mechanism that causes fast and more reluctant release of RRP vesicles. What causes these two release modes? One possibility is that fast and slow release are driven by different Ca^{2+} sensors (Goda and Stevens, 1994), with synaptotagmin-1 (Geppert et al., 1994; Voets et al., 2001) or its close homolog synaptotagmin-2 (Pang et al., 2006) representing the Ca^{2+} sensor for fast release. However, simulating the Ca^{2+}-uncaging data with a model that assumes two (sub)pools of readily releasable vesicles with different effective Ca^{2+} sensitivities (two-pool model) (Fig. 6) explained the observed intracellular Ca^{2+} sensitivities of the fast and the slow release component (Fig. 6*A*,*B*), but this model could not account for submaximal release, i.e., the surprising observation that the fast release component increased with $[Ca^{2+}]_i$ steps of increasing amplitudes (Figs. 4, 5). Interestingly, indications for submaximal release are also apparent in our previous work, in which maximal capacitance increases in response to Ca^{2+}-uncaging stimuli were only observed at >10 μM $[Ca^{2+}]_i$ (Wölfel and Schneggenburger, 2003, their Fig. 3).

Submaximal release of fusion-competent vesicles has first been reported in sea urchin eggs, in which low step-like elevations of $[Ca^{2+}]_i$ lead to the release of only a fraction of all fusion-competent vesicles, and an additional elevation of $[Ca^{2+}]_i$ triggered a new round of exocytosis (Blank et al., 1998). Blank et al. explained their data by assuming a distribution of Ca^{2+} sensitivities among fusion-competent vesicles. We think, however, that this is not a likely explanation for the submaximal release observed here. With a distribution of Ca^{2+} sensitivities among RRP vesicles, the release kinetics is expected to deviate from simple exponentials predicted by the one-pool model because, at each $[Ca^{2+}]_i$, a mix of various exponentials would result. Nevertheless, the RRP should eventually be depleted regardless of the amplitude of the $[Ca^{2+}]_i$ step. Indeed, in additional simulations (data not shown), an assumed Gaussian distribution of apparent Ca^{2+} sensitivities across the RRP (by varying the "fusion willingness," l_+), did not produce notable biphasic release or submaximal release of the fast release component.

It is therefore necessary to consider models in which the Ca^{2+} sensitivity of RRP vesicles drops after the onset of long-lasting or repetitive Ca^{2+} stimuli (a posteriori decrease of Ca^{2+} sensitivity). Previous work has proposed a posteriori mechanisms of a reduction in release probability, such as an inhibitory process that reduces the release probability of neighboring docked vesicles after a single vesicle release event (Stevens and Wang, 1995; Dobrunz et al., 1997) or adaptation of the vesicle fusion machinery to prolonged elevations of $[Ca^{2+}]_i$ (Hsu et al., 1996). Here, the reciprocal relationship between the fast and the slow release component must also be taken into account. It is conceivable that RRP vesicles all have a high Ca^{2+} sensitivity under resting conditions; this would explain the finding that $[Ca^{2+}]_i$ steps of high amplitudes (>30 μM) release a large fraction of the RRP in the fast release component (Fig. 5). During prolonged $[Ca^{2+}]_i$ stimuli of lower amplitude (5–10 μM), however, some vesicles are released with fast kinetics, whereas others might reach a distinct conformational state from which they can only be released more reluctantly, with an ~10- to 20-fold slower intrinsic release rate as apparent by the difference between fast and slow release rate over a large range of $[Ca^{2+}]_i$ (Fig. 6*B*). This explanation assumes that a conformational switch occurs in the vesicle fusion machinery of a given RRP vesicle after the onset of a Ca^{2+} stimulus, leading to an a posteriori decrease in the Ca^{2+} sensitivity. This idea has some similarities to adaptation of the vesicle fusion machinery to elevated $[Ca^{2+}]_i$ (Hsu et al., 1996), but Hsu et al. (1996) did not consider a transition from a fast to a slow release mode.

Functional implications

Submaximal release of fast-releasing vesicles was also observed during trains of AP-like stimuli, when different release probabilities were imposed by presynaptic voltage clamp (Fig. 7). Here, it showed up as an apparent pool size increase with increasing presynaptic release probability. We also observed an increased pool size in fiber stimulation experiments when the extracellular Ca^{2+} concentration was elevated from 2 to 4 mM in the presence of CTZ and γ-DGG (relative increase; 182 ± 11%; $n = 4$ cells; data not shown). These findings agree with the recent demonstration in hippocampal neurons that increasing the Ca^{2+} influx during train stimuli leads to increased apparent pool sizes and that a second slower component of depression likely corresponds to the release of reluctantly releasable vesicles (Moulder and Mennerick, 2005). This might be explained either by an increased coupling of SRP vesicles to AP-evoked release at increased Ca^{2+} influx (in the framework of a two-pool model) or else by a decreased entry of RRP vesicles into a reluctantly releasable state under conditions of high Ca^{2+} influx (in the framework of an a posteriori mechanism of reduced Ca^{2+} sensitivity). Regardless of the exact mechanism, we would argue that some RRP vesicles are released reluctantly because of a mechanism intrinsic to the vesicle fusion machinery based on our Ca^{2+}-uncaging data.

Submaximal release of fast-releasable vesicles might have interesting properties for information transfer at synapses. With submaximal release, the integrated synaptic weight during the onset of a brief high-frequency train (Fig. 7*A1*) will depend on the effective release probability of an RRP vesicle. Thus, presynaptic modulation of the amount of Ca^{2+} influx, for example after activation of presynaptic metabotropic receptors (Takahashi, 2005) or direct modulation of the release probability by the presynaptic munc-13/protein kinase C pathway (Lou et al., 2005; Basu et al., 2007), are expected to modulate the effective pool size. At some cortical synapses, on the other hand, long-term synaptic strengthening simply leads to a redistribution of synaptic weight

from late to early stimuli (Markram and Tsodyks, 1996), more similar to what is expected from simple pool depletion models. It is possible, therefore, that the degree of submaximal release differs between synapses, and it will be interesting to determine at which synapses submaximal release plays important roles in information processing.

References

Basu J, Betz A, Brose N, Rosenmund C (2007) Munc-13-1 C1 domain activation lowers the energy barrier for synaptic vesicle fusion. J Neurosci 27:1200–1210.

Blank PS, Cho M-S, Vogel SS, Kaplan D, Kang A, Malley J, Zimmerberg J (1998) Submaximal responses in calcium-triggered exocytosis are explained by differences in the calcium sensitivity of individual secretory vesicles. J Gen Physiol 112:559–567.

Bollmann J, Sakmann B, Borst J (2000) Calcium sensitivity of glutamate release in a calyx-type terminal. Science 289:953–957.

Borst JGG, Sakmann B (1996) Calcium influx and transmitter release in a fast CNS synapse. Nature 383:431–434.

Burrone J, Neves G, Gomis A, Cooke A, Lagnado L (2002) Endogenous calcium buffers regulate fast exocytosis in the synaptic terminal of retinal bipolar cells. Neuron 33:101–112.

Dobrunz LE, Huang EP, Stevens CF (1997) Very short-term plasticity in hippocampal synapses. Proc Natl Acad Sci USA 94:14843–14847.

Felmy F, Neher E, Schneggenburger R (2003) The timing of phasic transmitter release is Ca^{2+} dependent and lacks a direct influence of presynaptic membrane potential. Proc Natl Acad Sci USA 100:15200–15205.

Foster KA, Kreitzer AC, Regehr WG (2002) Interaction of postsynaptic receptor saturation with presynaptic mechanisms produces a reliable synapse. Neuron 35:1115–1126.

Geppert M, Goda Y, Hammer RE, Li C, Rosahl TW, Stevens CF, Südhof TC (1994) Synaptotagmin I: a major Ca^{2+} sensor for transmitter release at a central synapse. Cell 79:717–727.

Goda Y, Stevens CF (1994) Two components of transmitter release at a central synapse. Proc Natl Acad Sci USA 91:12942–12946.

Grynkiewicz G, Poenie M, Tsien R (1985) A new generation of Ca^{2+} indicators with greatly improved fluorescence properties. J Biol Chem 260:3440–3450.

Heinemann C, Chow RH, Neher E, Zucker RS (1994) Kinetics of the secretory response in bovine chromaffin cells following flash photolysis of caged Ca^{2+}. Biophys J 67:2546–2557.

Horrigan FT, Bookman RJ (1994) Releasable pools and the kinetics of exocytosis in adrenal chromaffin cells. Neuron 13:1119–1129.

Hsu S-F, Augustine GJ, Jackson MB (1996) Adaptation of Ca^{2+}-triggered exocytosis in presynaptic terminals. Neuron 17:501–512.

Kushmerick C, Renden R, von Gersdorff H (2006) Physiological temperatures reduce the rate of vesicle pool depletion and short-term depression via an acceleration of vesicle recruitment. J Neurosci 26:1366–1377.

Lindau M, Neher E (1988) Patch-clamp techniques for time-resolved capacitance measurements in single cells. Pflügers Arch 411:137–146.

Liu G, Choi S, Tsien RW (1999) Variability of neurotransmitter concentration and nonsaturation of postsynaptic AMPA receptors at synapses in hippocampal cultures and slices. Neuron 22:395–409.

Lou X, Scheuss V, Schneggenburger R (2005) Allosteric modulation of the presynaptic Ca^{2+} sensor for vesicle fusion. Nature 435:497–501.

Markram H, Tsodyks M (1996) Redistribution of synaptic efficacy between neocortical pyramidal neurons. Nature 382:807–810.

Matthews G (2001) Calcium/calmodulin: a synaptic antidepressant? Neuron 32:962–963.

Meinrenken C, Borst JGG, Sakmann B (2002) Calcium secretion coupling at calyx of Held governed by nonuniform channel-vesicle topography. J Neurosci 22:1648–1667.

Meyer AC, Neher E, Schneggenburger R (2001) Estimation of quantal size and number of functional active zones at the calyx of Held synapse by nonstationary EPSC variance analysis. J Neurosci 21:7889–7900.

Moulder KL, Mennerick S (2005) Reluctant vesicles contribute to the total readily releasable pool in glutamatergic hippocampal neurons. J Neurosci 25:3842–3850.

Neher E (1998) Vesicle pools and Ca^{2+}-microdomains: new tools for understanding their roles in neurotransmitter release. Neuron 20:389–399.

Neher E, Sakaba T (2001) Combining deconvolution and noise analysis for the estimation of transmitter release rates at the calyx of Held. J Neurosci 21:444–461.

Pang ZP, Sun JY, Rizo J, Maximov A, Südhof TC (2006) Genetic analysis of synaptotagmin 2 in spontaneous and Ca^{2+}-triggered neurotransmitter release. EMBO J 25:2039–2050.

Rozov A, Burnashev N, Sakmann B, Neher E (2001) Transmitter release modulation by intracellular Ca^{2+} buffers in facilitating and depressing nerve terminals of pyramidal cells in layer 2/3 of the rat neocortex indicates a target cell-specific difference in presynaptic calcium dynamics. J Physiol (Lond) 531:807–826.

Sakaba T (2006) Roles of the fast-releasing and the slowly releasing vesicles in synaptic transmission at the calyx of Held. J Neurosci 26:5863–5871.

Sakaba T, Neher E (2001a) Quantitative relationship between transmitter release and calcium current at the calyx of Held synapse. J Neurosci 21:462–476.

Sakaba T, Neher E (2001b) Calmodulin mediates rapid recruitment of fast-releasing synaptic vesicles at a calyx-type synapse. Neuron 32:1119–1131.

Scheuss V, Schneggenburger R, Neher E (2002) Separation of presynaptic and postsynaptic contributions to depression by covariance analysis of successive EPCSs at the calyx of Held synapse. J Neurosci 22:728–739.

Schikorski T, Stevens CF (2001) Morphological correlates of functionally defined synaptic vesicle populations. Nat Neurosci 4:391–395.

Schneggenburger R (2004) Ca^{2+} uncaging in nerve terminals. Imaging in neuroscience and development (Yuste R, Konnerth A, eds). Cold Spring Harbor, NY: Cold Spring Harbor Laboratory.

Schneggenburger R, Neher E (2000) Intracellular calcium dependence of transmitter release rates at a fast central synapse. Nature 406:889–893.

Schneggenburger R, Meyer AC, Neher E (1999) Released fraction and total size of a pool of immediately available transmitter quanta at a calyx synapse. Neuron 23:399–409.

Schneggenburger R, Sakaba T, Neher E (2002) Vesicle pools and short-term synaptic depression: lessons from a large synapse. Trends Neurosci 25:206–212.

Sorensen JB (2004) Formation, stabilization and fusion of the readily releasable pool of secretory vesicles. Eur J Physiol 448:347–362.

Stevens CF, Wang Y (1995) Facilitation and depression at single central synapses. Neuron 14:795–802.

Sun J-Y, Wu L-G (2001) Fast kinetics of exocytosis revealed by simultaneous measurements of presynaptic capacitance and postsynaptic currents at a central synapse. Neuron 30:171–182.

Takahashi T (2005) Dynamic aspects of presynaptic calcium currents mediating synaptic transmission. Cell Calcium 37:507–511.

Trommershäuser J, Schneggenburger R, Zippelius A, Neher E (2003) Heterogeneous presynaptic release-probabilities: functional relevance for short-term plasticity. Biophysical J 84:1563–1579.

Voets T (2000) Dissection of three Ca^{2+}-dependent steps leading to secretion in chromaffin cells from mouse adrenal slices. Neuron 28:537–545.

Voets T, Moser T, Lund P-E, Chow RH, Geppert M, Südhof TC, Neher E (2001) Intracellular calcium dependence of large dense-core vesicle exocytosis in the absence of synaptotagmin I. Proc Natl Acad Sci USA 98:11680–11685.

Wadiche JI, Jahr CE (2001) Multivesicular release at climbing fiber-Purkinje cell synapses. Neuron 32:301–313.

Wölfel M, Schneggenburger R (2003) Presynaptic capacitance measurements and Ca^{2+} uncaging reveal submillisecond exocytosis kinetics and characterize the Ca^{2+} sensitivity of vesicle pool depletion at a fast CNS synapse. J Neurosci 23:7059–7068.

Wu L-G, Borst JGG (1999) The reduced release probability of releasable vesicles during recovery from short-term synaptic depression. Neuron 23:821–832.

Xu J, Wu LG (2005) The decrease in presynaptic calcium current is a major cause of short-term depression at a calyx-type synapse. Neuron 46:633–645.

Yamashita T, Hige T, Takahashi T (2005) Vesicle endocytosis requires dynamin-dependent GTP hydrolysis at a fast CNS synapse. Science 307:124–127.